



OPEN ACCESS

EDITED BY

Q Wang,
Guangzhou University of Chinese
Medicine, China

REVIEWED BY

Kameni Poumeni Mireille,
University of Bamenda, Cameroon
Guanghui Chen,
Peking University Third Hospital, China
Sun Jingyi,
Shandong Provincial Hospital, China

*CORRESPONDENCE

Guoqing Tan
305215927@qq.com
Zhanwang Xu
xzw6001@163.com
Lingfeng Zeng
zenglf6768@163.com

SPECIALTY SECTION

This article was submitted to
Bone Research,
a section of the journal
Frontiers in Endocrinology

RECEIVED 28 April 2022

ACCEPTED 30 June 2022

PUBLISHED 02 August 2022

CITATION

Su H, Xue H, Gao S, Yan B, Wang R,
Tan G, Xu Z and Zeng L (2022) Effect
of *Rhizoma Drynariae* on differential
gene expression in ovariectomized
rats with osteoporosis based on
transcriptome sequencing.
Front. Endocrinol. 13:930912.
doi: 10.3389/fendo.2022.930912

COPYRIGHT

© 2022 Su, Xue, Gao, Yan, Wang, Tan,
Xu and Zeng. This is an open-access
article distributed under the terms of
the [Creative Commons Attribution
License \(CC BY\)](https://creativecommons.org/licenses/by/4.0/). The use, distribution
or reproduction in other forums is
permitted, provided the original author
(s) and the copyright owner(s) are
credited and that the original
publication in this journal is cited, in
accordance with accepted academic
practice. No use, distribution or
reproduction is permitted which does
not comply with these terms.

Effect of *Rhizoma Drynariae* on differential gene expression in ovariectomized rats with osteoporosis based on transcriptome sequencing

Hui Su¹, Haipeng Xue², Shang Gao¹, Bingham Yan¹,
Ruochong Wang³, Guoqing Tan^{2*}, Zhanwang Xu^{1,2*}
and Lingfeng Zeng^{4*}

¹First Clinical Medical College, Shandong University of Traditional Chinese Medicine, Jinan, China, ²Affiliated Hospital of Shandong University of Traditional Chinese Medicine, Jinan, China, ³College of traditional Chinese medicine, Beijing University of Traditional Chinese Medicine, Beijing, China, ⁴The 2nd Affiliated Hospital of Guangzhou University of Chinese Medicine, Guangzhou, China

Osteoporosis is increasingly becoming a serious problem affecting the quality of life of the older population. Several experimental studies have shown that Chinese medicine has a definite effect on improving osteoporosis. Based on transcriptome sequencing, we analyzed the differential gene expression and mechanism of the related signaling pathways. Fifteen rats were randomly divided into an experimental group, a model group, and a sham surgery group. The rat model for menopausal osteoporosis was established using an ovariectomy method. One week after modeling, the experimental group was administered (intra-gastric administration) 8.1 g/kg of *Rhizoma drynariae*, whereas the model and sham groups received 0.9% saline solution twice daily for 12 weeks. Subsequently, the rats were sacrificed, and the left femur of each group was removed for computerized tomography testing, while right femurs were used for hematoxylin and eosin staining. High-throughput RNA sequencing and functional and pathway enrichment analyses were performed. Comparing the gene expression between the experimental and model groups, 149 differential genes were identified, of which 44 were downregulated and 105 were upregulated. The criteria for statistical significance were $|\log_2 \text{Fold Change}| > 1$ and $P < 0.05$. Gene ontology analysis showed that the differentially expressed genes were enriched in cell component terms such as cell part and outer cell membrane part, and the genes were associated with cell process, biological regulation, metabolic processes, DNA transcription, and catalytic activity. Enrichment analysis of Kyoto Encyclopedia of Genes and Genomes pathways showed significantly enriched pathways associated with systemic lupus erythematosus, herpes simplex infection, circadian rhythm, vascular smooth muscle contraction, the AGE-RAGE signaling pathway in diabetic complications, and the TNF, Apelin, and Ras signaling pathways. Our results revealed that the *Npas2*, *Dbp*, *Rt1*, *Arntl*, *Grem2*, *H2bc9*, *LOC501233*, *Pla2g2c*, *Hpgd*, *Pde6c*, and *Dner* genes, and the circadian rhythm, lipid metabolism,

inflammatory signaling pathway, and immune pathways may be the key targets and pathways for traditional Chinese medicine therapy of *Rhizoma Drynariae* in osteoporosis.

KEYWORDS

Rhizoma Drynariae, ovariectomized, rats, osteoporosis, transcriptome sequencing

1 Introduction

Osteoporosis, a disease with increased bone fragility and risk of fracture due to decreased bone formation and increased destruction of bone resorption (1, 2), is progressively becoming a serious problem affecting the quality of life of the older population.

In the study of the pathophysiology of osteoporosis, we have found that factors associated with bone strength and damage include a weakened microstructure and tissue of the trabecular bone and decreased bone formation with excessive bone resorption. These factors are closely related to age and changes in estrogen levels (3). In terms of bone metabolism, the pathogenesis of osteoporosis lies in the imbalance between bone resorption and bone formation.

Current drug treatments for osteoporosis include basic supplements (mainly calcium and vitamin D), bone absorption inhibitors [such as bisphosphonates, calcitonins, and selective estrogen receptor modulators (4)]; and bone formation promoters [including thyroxine (5)]. Additionally, treatment with strontium ranelate has a bidirectional effect, i.e., inhibiting bone resorption and promoting bone formation (6).

Postmenopausal osteoporosis, also known as primary osteoporosis, is common in older, postmenopausal women, presenting bone pain, adverse limb movement, and an increased risk of bone fracture. Estrogen deficiency is the major cause of postmenopausal bone loss, while older age, smoking, chronic disease, and other related illnesses and drugs are additional causes (7, 8).

Chinese herbal medicine has an apparent effect on osteoporosis, as it can ameliorate bone health through multiple targets and pathways (9). *Rhizoma Drynariae* is a traditional Chinese medicine that improves bone by promoting trauma recovery (10). Although there are some studies on the effect of bone repair in osteoporosis (11, 12) (13), the mechanisms and targets are difficult to elucidate due to their complex

composition (14, 15). Here, we aim to explore the specific action of target genes using transcriptome sequencing technology and reveal the molecular mechanisms related to the efficacy of *Rhizoma Drynariae*. The identification of these mechanisms will promote the use of Chinese herbal medicine in the clinical treatment of osteoporosis.

2 Materials and methods

2.1 Animals and medicines

Female Sprague-Dawley rats (6-weeks-old, weight 200–220 g) were purchased from Beijing Vital River Laboratory Animal Technology Co., Ltd. The feeding environment was clean and well ventilated, and water was freely available. All animals were housed at the SPF Grade Animal Experimental Center of Shandong Provincial Hospital of Traditional Chinese Medicine at 25°C with a constant humidity of 50% for 12 h per day and given a standard diet. The experimental animals were bred for 7 d, and 15 rats were divided into the experimental group (OVXDF), the model group (OVX), and the sham operation group (SHAM). In the OVXDF and OVX groups, a preoperative diet was not provided for 12 h, and intraperitoneal pentobarbital sodium (10g/L) was used for anesthesia. The OVXDF group was subjected to surgical resection of their bilateral ovaries, and only small peripheral adipose tissue around the ovary was removed in the SHAM group (16). After the operation, an intramuscular injection of penicillin (50,000 U/d) was administered to prevent infection. On the seventh day after the operation, we administered *Rhizoma Drynariae* to the rats by intragastric administration.

The preparation of drug decoction was followed the preliminary preparation protocol of our research group (17, 18). Granules of *Rhizoma Drynariae* was purchased from the pharmacy of the Affiliated Hospital of Shandong University of Traditional Chinese Medicine. Next, 100 g of *Rhizoma Drynariae* was placed in a pot distilled with water and concentrated to 100 mL. Liquid *Rhizoma Drynariae* (1 g/mL) was obtained and stored at 4°C.

Following the animal dose conversion formula (19), *Rhizoma Drynariae* gavage was administered at a potency of 8.1 g/kg to the OVXDF group, and 0.9% saline solution was

Abbreviations: CT, computerized tomography; DEG, differentially expressed gene; ECM, extracellular matrix; H&E, hematoxylin and eosin; GO, gene ontology; KEGG, Kyoto Encyclopedia of Genes and Genomes; PPI, protein-protein interaction; STRING, Search Tool for the Retrieval of Interacting Genes; T2DM, type 2 diabetes.

administered to the OVX and SHAM groups twice daily for 12 weeks. The experimental procedures were conducted in accordance with the management and use of experimental animal guidelines of the Shandong Provincial Hospital of Traditional Chinese Medicine, and the study was approved by the ethical review committee (Affiliate hospital of Shandong University of Traditional Chinese Medicine 2021-26).

2.2 Bone mineral density measurements and micro-CT of bone

Rats were sacrificed following a sodium pentobarbital overdose (60mg/kg) (20), and bilateral femurs were removed. The left femurs were subjected to computerized tomography (CT) testing with a tone-beam bench-top, miniature CT device (μ CT80, Scanco Medical, Brüttisellen, Switzerland), and images were analyzed using μ CT80 Evaluation Program v6.51 (Scanco Medical). Proliferous bones with the distal femur 1 mm above the growth plate were selected after scanning a volume-of-interest restricted to the internal femur region. The trabecular and cortical bones were extracted by drawing free-form contour lines using the CT analyzer software. Using the microstructure of cancellous bone, 3D images were obtained by multiplane reorganization. The region of interest was analyzed using the CT Analyser v1.18.8.0 (Bruker, Germany). Using the uniform parameters, bone mineral density (BMD; g/cm³), bone volume fraction [BV/total volume (TV); %], bone surface area volume fraction (BS/TV; 1/mm), and the number of trabecular bone (Tb.N; 1/mm) were calculated.

2.3 Hematoxylin and eosin staining and TRAP staining

2.3.1 HE staining

The right femur of each group was taken, cleaned and fixed in 10% formaldehyde solution for 48 h, washed in running water and distilled water for 24 h. The specimen was decalcified, and the decalcification was stopped after 3~4 h. The alkaline solution was washed for 12h, then dehydrated, transparent and wax, respectively, embedded and sliced in paraffin, and the drying time was about 10~15 min.

2.3.2 TRAP staining

The right femoral paraffin sections of each group were dewaxed for 5 to 10 min for 5min with absolute ethanol, 90% ethanol, and 70% ethanol for 2min each. After washing and drying naturally for 2min, the fixative was fixed for 30s~3min at room temperature, stained with appropriate staining solution, covering the tissue, placed in a 37°C temperature box, and washed for 45~60min. Compound staining was performed for

5 to 8 min or methyl green staining for 2 to 3 min. Finally, it was washed, dried and micro examine.

2.4 High-throughput RNA sequencing

Total RNA was extracted from the bone tissue samples selected from each group after using TRIzol (Invitrogen, CA, USA), Samples are sequenced on the platform to get image files, which are transformed by the software of the sequencing platform, and the original data is generated. we use Cutadapt (v1.15) software to filter the sequencing data to get high quality sequence for further analysis. Finally obtained the expression of differential genes between the OVX group and OVXDF group.

2.5 Differential expression analysis and hierarchical clustering

Differential gene expression was analyzed using DESeq (R package). Differentially expressed genes (DEGs) were selected with $|\log_2 \text{Fold Change}| > 1$ and $P < 0.05$ as criteria for statistical significance. DEGs were represented using graphs to calculate the number of upregulated and downregulated DEGs in each comparison group. Volcano maps showing gene distribution of the DEGs were obtained using ggplot2 (R package). Two-way clustering analysis of the union and samples of DEGs across all comparison groups was performed using Pheatmap (R package).

2.6 Functional and pathway enrichment analysis

Gene ontology (GO) enrichment analysis using topGO ($P < 0.05$) was performed to determine the significantly enriched GO terms for DEGs and identify their main biological functions. Kyoto Encyclopedia of Genes and Genomes (KEGG) pathway enrichment analysis was performed using the clusterProfiler v3.4.4 software, focusing on significantly enriched pathways with $P < 0.05$.

2.7 Protein-protein interaction analysis

Protein interaction analysis was performed employing the Search Tool for the Retrieval of Interacting Genes (STRING) database (<https://string-db.org/>) to reveal the functional relationship between the target genes. When PPI information for this species was included in the STRING database, PPI action pairs containing DEGs and scores > 0.95 were screened based on the results of the DEG analysis. Differential gene correlation was also assessed by visual analysis using the Cytoscape v3.7.2 software.

2.8 Validation of RNA-seq results using qRT-PCR

Bone tissue was taken 50 mg to 1 mL Trizol using liquid nitrogen, 0.2 mL of chloroform, total RNA was extracted by Trizol, RNA concentration, purity and integrity, and cDNA. The corresponding PCR reaction amplification system (25 L) was added, PCR thermocycler amplification, amplification conditions: 95°C pre-denaturation for 3 min; 95°C was denatured for 20s, 60°C annealed for 15s, 72°C extended for 30s, and amplified in 45 cycles. The last 72°C was extended for 1 min. For SDS polyacrylamide gel electrophoresis, the image analysis software analyzed the band density, and the relative expression of the genes was calculated using the $2^{-\Delta\Delta Ct}$ method. Five DEGs with different expression patterns were randomly chosen to validate the accuracy of the transcriptome sequencing results, qRT-PCR was verified using actin as the internal reference. The primers used are listed below (Table 1).

2.9 Statistical analysis

All the data were expressed as the mean \pm standard deviation. An independent sample t-test evaluated the significant differences between two groups using SPSS v24.0 (SPSS, IL, USA), and $P < 0.05$ was considered significant. GraphPad Prism v7.0 (GraphPad Software, CA, USA) was utilized. All assays were conducted three times or more.

3. Results

3.1 Rat bone density measurement and micro-CT

The results showed that the bone mineral density of the OVX group was significantly lower than the SHAM group ($P < 0.05$). In contrast, the bone mineral density of the OVXDF group was significantly higher than that of the OVX group ($P < 0.05$). Moreover, the bone volume score (BV/TV), surface area volume fraction (BS/TV), and number of trabecular bones (Tb.N) for the

OVXDF and SHAM groups were significantly higher than those of the OVX group ($P < 0.05$; Figure 1).

Micro-CT images showed that the trabecular bone in the OVX group had a sparse microstructure. However, in the OVXDF group, the trabecular bone is large, with dense arrangement and small gaps, indicating that the Rhizome Drynaria improves the trabecular microstructure of the femur (Figure 2).

3.2 H&E staining and TRAP staining

The femurs in the OVX group were thinning and decreasing, with apparent osteoporosis characteristics such as fractures and increased bone resorption holes. Rats in the SHAM group had abundant cancellous bone, many bony trabeculae, a tight arrangement, complete bone tissue structure, and a thick and uniform wall. In the OVXDF group, the structure of the femoral trabecular bone was relatively complete, the texture was tightly arranged, the bone trabecular connectivity was better, and the wall thickness was denser compared with the OVX group. Osteoclasts were stained red in TRAP staining, and the staining result showed that compared with the SHAM group, the OVX group osteoclasts were more numerous and widely distributed, while compared with the OVX group, the OVXDF group osteoclasts were fewer and concentrated. Overall, the state of the trabecular and cancellous bones in the OVXDF group was superior to that of the OVX group (Figure 3).

3.3 High-throughput RNA sequencing

A total of 17,591 transcriptome mRNA was obtained from the OVXDF and OVX groups. Based on the results of the differential gene analysis, 416 DEGs were identified in the OVXDF, OVX, and SHAM groups, and the mutual relationship was displayed in a Venn diagram (Figure 4). In comparing gene expression between the OVXDF and OVX groups, 149 DEGs were identified, of which 44 were down regulated and 105 were upregulated. Further screening of the most significant gene expression showed 12 DEGs, including 8

TABLE 1 Primers used for RT-qPCR test.

Gene	Forward Primer	Reverse Primer
Grem2	CCTGAAGAGTGACTGGTGCAAGAC	GTGTCGTGGGATGTAGAAGGAGTTG
Dbp	CACCGCTTCTCAGAGGAGGAATTG	CCTCTGGCTGCTTCATTGTTCTTG
Dner	TGGAGCCCTGTGTGTAGCCTTC	CGTTGCTGAACACTCACTGTCAATGC
Arnt1	AACCATTGTCCAGCCGTCATCTTC	AACCATTGTCCAGCCGTCATCTTC
npas2	GCTGATGTTGGAGGCGTTAGATGG	ATGTCGAGGAGAGGCGGTGATG
GAPDH	GAACATCATCCCTGCATCCA	GCCAGTGAGCTCCCGTTCA

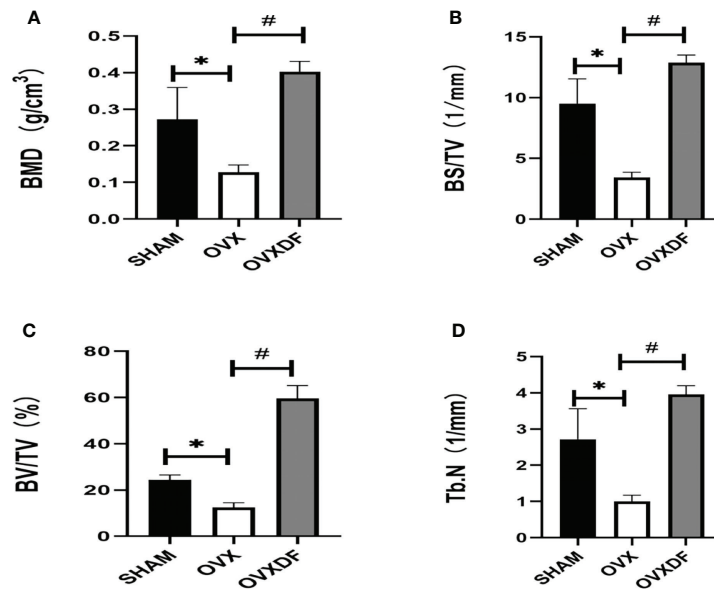


FIGURE 1
 Bone parameter values of Micro-CT. **(A)** The BMD indicates the bone mineral density in the bone tissue of the region of interest. **(B)** Bone surface area and tissue volume ratio (BS/TV) can indirectly reflect the amount of bone mass. **(C)** Bone body and fraction (BV/TV) are commonly used in the evaluation of cortical and cancellous bone mass. **(D)** Number of trabecular bone (Tb.N) to evaluate the spatial morphological structure of trabecular bone. **P*<0.05 versus SHAM group, #*P*<0.05, versus OVXDF group, *n* = 3 per group, Data were shown as mean ± sd.

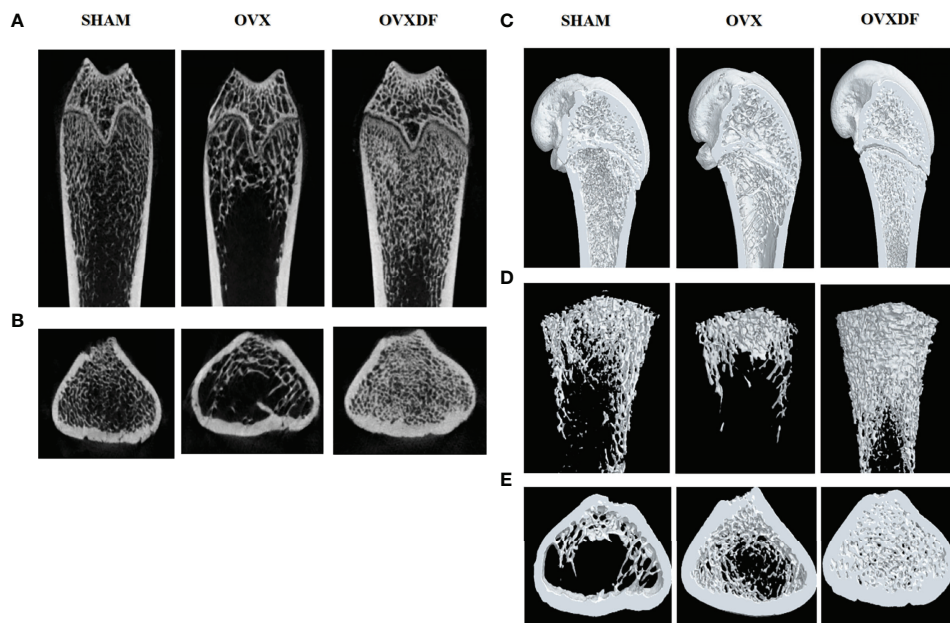
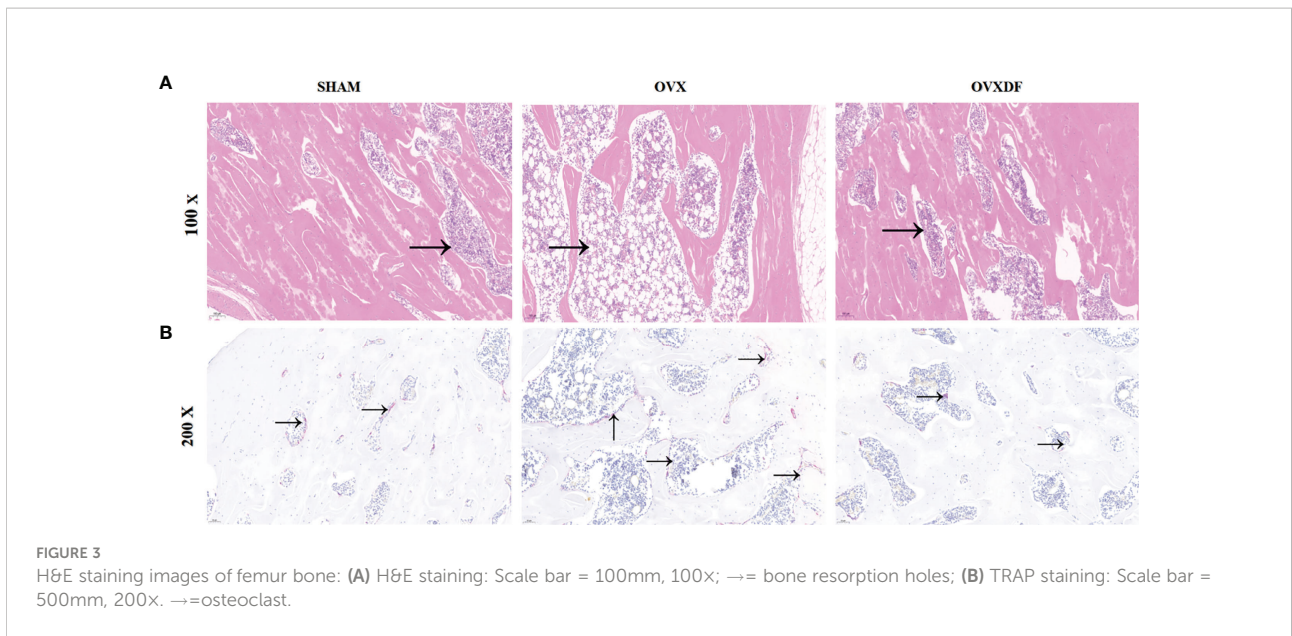


FIGURE 2
 Micro-CT images of the femur. **(A, B)** 2D images in three groups of the distal femur (scale bars, 1 mm). **(C–E)** 3D images in three groups of the proximal femur (scale bars, 1 mm).



upregulated and 4 downregulated genes (Table 2). Moreover, we performed a two-way clustering analysis of the acquired genes between the three groups (Figure 4). In comparing gene expression between the SHAM and OVX groups, 227 DEGs were identified, of which 110 were upregulated and 127 were downregulated. These details were presented as column diagrams and volcano charts (Figure 4).

3.4 Functional and pathway enrichment analysis

3.4.1 GO enrichment analysis of the DEGs

Enrichment analysis of DEGs (Figure 5) from the OVXDF and OVX groups showed that 149 DEGs were collectively enriched in 362 molecular functions, 253 cellular components,

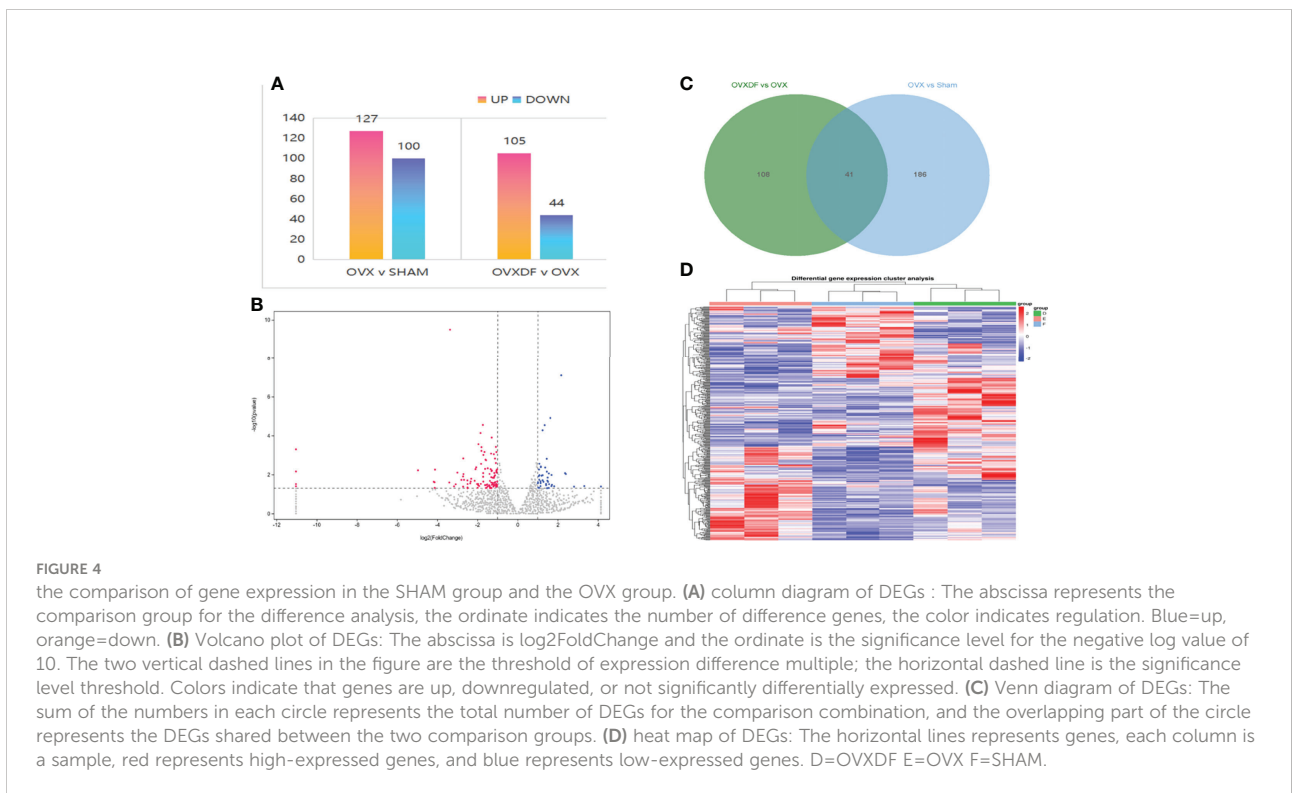


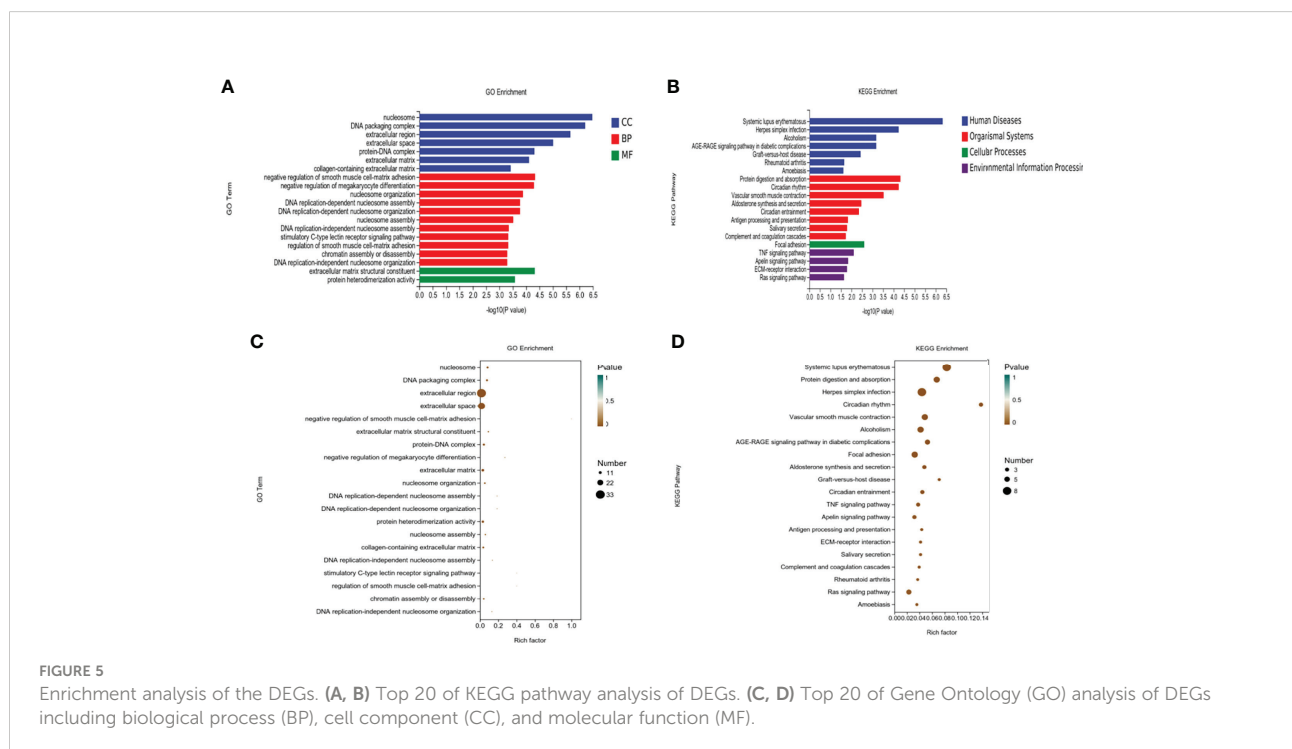
TABLE 2 12 significantly DEGs in OVXDF group and OVX group.

Name	log2FoldChange	pval	Regulation
Npas2	3.37324286	3.16E-10	up Regulation
Dbp	-2.177429033	7.93E-08	down Regulation
LOC103690108	11.03293695	0.000499027	up Regulation
Arntl	2.702206184	0.001462716	up Regulation
Grem2	-2.060425268	0.004194338	down Regulation
H2bc9	2.094632641	0.005218957	up Regulation
LOC501233	4.110331215	0.00549491	up Regulation
Pla2g2c	4.958704937	0.005965812	up Regulation
Hpgd	2.998655062	0.007817667	up Regulation
Pde6c	-2.366381804	0.008314784	down Regulation
AABR07065750.2	-2.405047687	0.009304366	down Regulation
Dner	2.691923189	0.009380164	up Regulation

| log2FoldChange |> 2 with significant P-value <0.01.

and 2478 biological processes. Considering $P < 0.05$ as the criterion for significant enrichment, the top enrichment scores were ranked in cell part, outer cell membrane part, cell process, biological regulation, metabolic process, DNA transcription, and catalytic activity. DEGs enriched in molecular function included extracellular matrix (ECM) structural constituent and protein heterodimerization activity. DEGs enriched in cellular component terms, facilitated by the major enrichment in the nucleosome, included DNA and protein-DNA packaging complex, extracellular space, and collagen-containing ECM. Furthermore, the DEGs were involved in biological processes

such as negative regulation of smooth muscle cell-matrix adhesion, negative regulation of megakaryocyte differentiation, nucleosome organization, DNA replication-dependent and -independent nucleosome assembly, stimulatory C-type lectin receptor signaling pathway, and chromatin assembly or disassembly. Regulation of smooth muscle and cell-matrix adhesion contribute a large proportion of the biological process classification and changes in both states are closely related to the aging process. Whether the appearance of vascular calcification or cell-matrix adhesion affects the Wnt signaling pathway, they all cause bone loss to some extent. The



outer part of the cell membrane accounted for the most proportion of DEGs in the cell group classification. In the molecular function classification, ECM structural constituent, mainly by protein heterodimerization activity, can promote stem cell proliferation and maturation, the formation of matrix scaffold, and bone remodeling by bone-forming cells. It has been shown that[] changes in the functional properties of the ECM may be involved in diseases such as osteoporosis and oral bone loss.

3.4.2 KEGG enrichment analysis

DEGs from the OVXDF and OVX groups were mapped to the KEGG pathway database for enrichment analysis (Figure 5), obtaining 165 signaling pathways ($P < 0.05$), with 110 downregulated and 118 upregulated pathways. Top-scoring pathways included systemic lupus erythematosus, herpes simplex infection, alcoholism, the AGE-RAGE signaling pathway in diabetic complications, and graft-versus-host disease. The diseases associated with the DEGs included rheumatoid arthritis, amoebiasis, and organismal systems. Moreover, the DEGs were strongly correlated with protein digestion and absorption, circadian rhythm, vascular smooth muscle contraction, aldosterone synthesis and secretion, antigen processing and presentation, salivary secretion, complement and coagulation cascades, and cellular processes. The most enrichment was in focal adhesion and environmental information processing. Furthermore, the DEGs were

primarily enriched in inflammatory immune signaling pathways such as the TNF, Apelin, and Ras signaling pathways and ECM-receptor interaction.

3.4.3 PPI network related to DEGs

DEGs from the OVXDF group were analyzed using the STRING data (<https://string-db.org/>) and imported into Cytoscape v3.7.2. The results showed 130 nodes and 111 edges, with an average node degree of 1.71. Genes with a large correlation between them were Col1a1 (collagen type I alpha 1 chain; degree = 12), Edn1 (endothelin 1; degree = 10), Mmp3 (matrix metalloproteinase 3; degree = 10), Serpine1 (serpin family E member 1; degree = 9), Acta2 (actin alpha 2; degree = 8), Eln (elastin; degree = 8), Ciart (circadian associated repressor of transcription; degree = 7), Arntl (aryl hydrocarbon receptor nuclear translocator-like; degree = 6), Npas2 (neuronal PAS domain protein 2; degree = 6), and Sox10 (SRY-box transcription factor 10; degree = 6) (Figure 6). Related genes were mostly enriched in the circadian rhythm, protein digestion and absorption, and the AGE-RAGE signaling pathway in diabetic complications (Figure 6).

3.5 Results of qRT-PCR

Following our transcriptomic sequencing results, five DEGs with apparent upregulation and downregulation were selected as

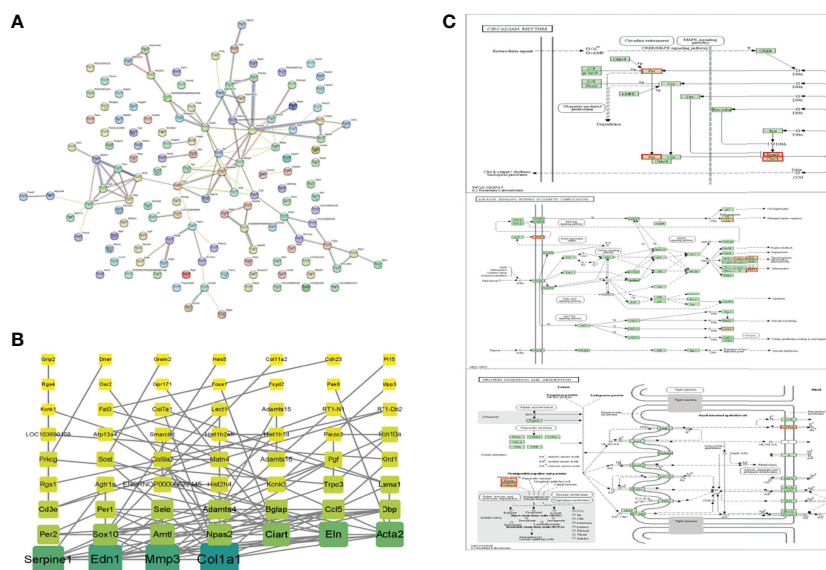


FIGURE 6
PPI networks of DEPs. (A) STRING data base (<https://string-db.org/>), Network nodes represents proteins, Edges represents protein-protein associations (B) Cytoscape3.7.2, Color and rectangular area are proportional to correlation and the darker color, the larger rectangular area and the greater correlation of DEPs. (C) top-ranked KEGG pathway based on the association degree analysis of DEPs. DEPs were marked in red. \Circadian rhythm.\Protein digestion and absorption. \AGE-RAGE signaling pathway in diabetic \complications.

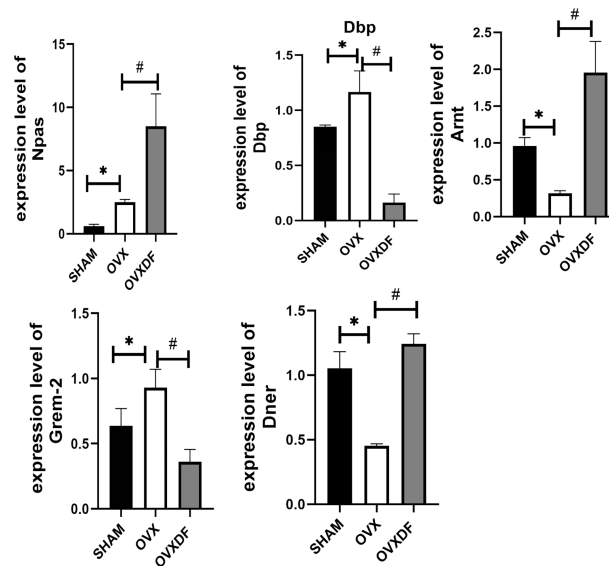


FIGURE 7

RT-qPCR results indicated that expression level of Npas2, Dbp, Arntl, Grem2 and Dner. * $P < 0.05$ versus sham group, # $P < 0.05$, versus OVX groups, $n = 3$ per group, Data were shown as mean \pm SD.

qRT-PCR validation targets, namely Npas2, Dbp, Arntl, Grem2, and Dner. Dbp was significantly upregulated in the OVXDF group compared with that in the OVX group. However, the expression of Npas2, Arntl, Grem2, and Dner was significantly downregulated. These results were consistent with our RNA-seq results, thus reaffirming them (Figure 7).

4. Discussion

In this study, we aimed to identify DEGs and their expression patterns for promoting bone repair in osteoporosis and further reveal the specific mechanism of genes in osteoporosis treatment through transcriptomic analysis of osteoporosis model rats (OVX) and experimentally treated osteoporosis rats (OVXDF). A total of 149 DEGs were identified between the two groups. The 10 most altered DEGs were Npas2, Dbp, RT1, Arntl, Grem2, H2bc9, LOC501233, Pla2g2c, Hpgd, Pde6c, and AABR07065750. These may be a potential target for treatment in ovariectomized rats with osteoporosis. We confirmed the positive role of Rhizoma Drynariae in improving osteoporosis by an experimental analysis of rat femoral tissue.

Combined with the results of the DEG analysis, we found that DEGs involved in Rhizoma Drynariae regulation are mainly related to the circadian rhythm, lipid metabolism-related diseases, osteoporosis disease, inflammation, and tumors. Osteoporosis treatment with Rhizoma Drynariae can play a significant role through multiple pathways, and we confirmed

that the Ras signaling pathway is important to regulate bone homeostasis and bone formation (21). Ras signaling combines with the downstream ERK signaling to promote osteoblast differentiation and bone formation during early skeletal development (22). The study by Peng (23) used miR-483-5p to down regulate Ras signaling by inhibiting RPL31 expression, resulting in the inhibition of osteogenic differentiation. Furthermore, Chen et al. (24) showed that the Apelin signaling pathway can activate mitophagy in bone marrow-derived mesenchymal stem cells, improve oxidative stress, and promote osteogenic function. One study (25) demonstrated that the Wnt/ β -catenin pathway may be the link between Apelin-13 and bone mineral density, but its precise role in bone metabolism is currently unknown.

The mechanisms of the inflammatory signaling and immune pathways in osteoporosis have been widely studied. Our analysis confirmed that Rhizoma Drynariae could regulate the tumor inflammatory pathway by changing the levels of inflammatory factors and reducing the inflammatory response to regulate the immune status. The prostaglandin dehydrogenase gene Hpgd also plays a role in tumor development and inflammation (26). In our enrichment analysis, differential genes, including H2bc9 and AABR07065750.2, were mostly associated with immune system diseases such as systemic lupus erythematosus, rheumatoid arthritis, and herpes simplex infection; the release of inflammatory cytokines and autoantibody production during the disease development leads to local and systemic bone loss (27). The use of drugs such as glucocorticoids in their treatment also exacerbates the risk of osteoporosis. Moreover, the National

Institutes of Health has identified graft-versus-host disease as a high-risk factor for osteoporosis (28) as the induced changes in the immune system lead to bone destruction. The inflammatory TNF signaling pathway was clearly expressed in the present analysis. A recent study revealed that tumor necrosis factor (TNF) directly enhances RANKL expression and promotes osteoclast formation (29). In bone metabolism (30), multiple target genes on the TNF pathway regulate osteoclast differentiation, thereby regulating physiological bone remodeling and participating in the pathogenesis of various bone diseases, such as osteoporosis and bone loss under inflammatory conditions. The ECM-receptor interaction pathway is mainly associated with cell communication, proliferation, and adhesion (31). At present, this pathway is primarily a marker for cancer and malignant tumors (32). However, a study (33) showed that the ECM-receptor interaction pathway may play a role in the impaired fracture healing of osteoporotic mice and is considered one of the causes of bone non-union (34).

Notably, multiple key genes associated with the circadian rhythm were significantly expressed in our results, including *Arntl*, *Npas2*, *Dbp*, *Per1*, and *Per2*. Our analysis confirmed the important role of the circadian rhythm in osteoporosis and the positive regulatory effect of *Rhizoma Drynariae*. Circadian rhythms are controlled by a molecular clock system located in the suprachiasmatic optic chiasmus (central clock) and the peripheral tissue (peripheral clock). Some studies have revealed that the disruption of circadian rhythms can lead to bone remodeling disorders and eventually osteoporosis because various bone regulatory growth factors are associated with clock genes (35). Fu (36) showed that the circadian rhythm is transmitted to peripheral osteoclasts and proved the role of clock genes in osteoclasts by extracting mRNA from the femur at different time periods and then analyzing the expression of osteoclast-related genes and clock genes. Osteoclast-related genes, such as *Ctsk* and *Nfatc1*, show distinct circadian rhythms.

Npas2, also known as neuronal PAS domain protein 2, is also recognized as a tumor suppressor (37). It has been shown that *Npas2*, as one of the core circadian rhythm genes, can play a role in cell development by regulating DNA-related genes. In one study, *NPAS2* was found to show high expression in a human fibrosis specimen and in a mouse fibrosis model (38). It indicates the profibrotic role of *Npas2*. A study of Morinaga (39) showed, after the placement of titanium biomaterial in mice, mice were found to be in a state of accelerated bone integration, where *NPAS2* expression was up regulated, revealing that *NPAS2* may be a possible mechanism of action involved in bone metabolism as a circadian gene *in vivo*. *NPAS2* usually cooperates with *Arnt-1* (*BMAL1*) to regulate the transcription of circadian genes. *BMAL1* also acts as a core component gene of circadian rhythms, and increasing evidence indicates that a key role of *BMAL1* in bone development can promote fracture healing and improve bone. Animal experiments confirm that when *BMAL1* receives inhibition, bone and cartilage development is hindered and thus caused by a decrease in bone mass

(40). Bunker showed that the *Bmal1*-null mice exhibit reduced bone mineral density and muscle strength. Cytomolecular experiments found that *BMAL1* exhibited a synergistic effect on the proliferation and differentiation of BMSC, and *BMAL1* deficiency inhibited osteoblast and chondrocyte differentiation while promoting the differentiation and formation of osteoclasts and increasing bone resorption (41, 42). Therefore, our experiment suggests the mechanism of action of the circadian rhythm in osteoporosis and the positive regulatory effect of *Rhizoma Drynariae*.

Previous findings show that *DBP* in omental adipose tissue has low expression in subcutaneous adipose tissue in patients with type 2 diabetes mellitus (T2DM), confirming its involvement in regulating the expression of genes related to lipid metabolism (43). As the major carrier protein of vitamin D metabolites, *DBP* is able to maintain calcium homeostasis through the targeted transport of vitamin D. Current studies have shown that *DBP* can be activated to (*DBP-MAF*) and then directly activate osteoclasts to promote bone resorption (44).

In this analysis, it was found that many genes about fat metabolism were also significantly expressed in differential genes and enriched pathways. It shows a positive regulatory role of *Rhizoma Drynariae* in regulating osteogenic differentiation and fat differentiation. *Gremlin-2*, a key bone morphogenetic protein (*GREM2*) (*BMP*) antagonist, can competitively bind *BMP* receptors to regulate the activity of *BMP* ligands, thus it plays a crucial role in regulating bone homeostasis (45). In the Yu Feng's study (46) showed that the *GREM2* gene polymorphisms were positively associated with the risk of osteoporosis in postmenopausal women. It has been shown that *GREM2* negatively regulates osteoblast differentiation by participating in the regulation of the *Wnt/catenin* signaling pathway (47). In the analysis of our experimental, the results also found that the significant regulation of *GREM2* occurs with the involvement of *Wnt/catenin*.

Several genes related to lipid metabolism, such as *HPGD* and *DNER*, were also confirmed to be significantly regulated in this analysis. It shows that *Rhizoma Drynariae* can regulate proteins and pathways related to lipid metabolism, improve the anti-oxidative stress resistance, thus promoting osteogenic expression and reversing osteoporosis.

Lisa et al. (48) showed the PPAR-induced *HPGD* expression in visceral adipose tissue (VAT) Treg cells. The conditional deletion of *Hpgd* in murine Treg cells causes local inflammation and systemic insulin resistance. Patients with type 2 diabetes exhibit reduced *HPGD* expression in Treg cells. These data suggest that *HPGD* is likewise involved in adipose tissue homeostasis. *Dner* acts as a Notch and EGF-related receptor (49), playing an important role in the adipogenic differentiation of human adipose tissue-derived mesenchymal stem cells. Studies revealed that a specific siRNA knockdown of *Dner*, eventually leads to increased adipose differentiation (50, 51). Wang (52) showed that Positive correlation between *DNER* and *Wnt/catenin* signaling. We speculate that *DNER* also promotes osteogenesis. Previous studies (53) found that *DNER*

expression was found to affect the expression of pathway genes in pancreatic cells, Reduce the occurrence of lipidation.

It also shows that osteoporosis is closely linked to T2DM. The AGE-RAGE signaling pathway is important in diabetes complications, including reduced bone mineral density and impaired bone quality. Our study confirmed that AGE-RAGE signaling has a role in promoting increased osteogenic function in bones (54). Moreover, the effects of *Rhizoma Drynariae* on the AGE-RAGE signaling pathway and lipid metabolism-related pathways have been extensively studied. In addition to T2DM, the diseases related to *Rhizoma Drynariae* regulation were also correlated with alcoholism and amoebiasis.

Although previous bioinformatics studies have been carried out on the effect of *Rhizoma Drynariae* in postmenopausal osteoporosis (15), no further verification has been conducted. In our DEG analysis, we have verified that *Rhizoma Drynariae* in osteoporosis model rats occurs through multiple pathways and targets. However, this study is limited by its small sample size, the difficulty of RNA extraction from bone tissue, and some errors that may affect the experimental results to a certain extent. Although the mechanisms of Chinese herbal medicine in the treatment of osteoporosis have been widely studied, the lack of a more comprehensive analysis necessitates further research. In this regard, transcriptome analysis can broaden the scope of research and provide new directions to these studies.

Data availability statement

The original contributions presented in the study are publicly available. This data can be found here: <https://www.ncbi.nlm.nih.gov/bioproject/PRJNA862708>, Accession: PRJNA862708; ID: 862708.

Ethics statement

The animal study was reviewed and approved by Affiliate Hospital of Shandong University. Written informed consent was

obtained from the owners for the participation of their animals in this study.

Author contributions

ZX, GT, and HS designed and developed the experiments. HS and HX prepared the draft of the manuscript. HS, HX, GT, ZX, SG, BY and RW participated in all the experiments. HS, BY, RW and HX analyzed the data and drafted the manuscript. HX, GT, LZ, and ZX supervised all research and revised the manuscript. All authors contributed to the article and approved the submitted version.

Funding

This study was funded by National Natural Science Foundation of China (82174410); Natural Science Foundation of Shandong Province, ZR2020KH011 Natural Science Foundation of Shandong Province, ZR2020MH362.

Conflict of interest

The authors declare that the research was conducted in the absence of any commercial or financial relationships that could be construed as a potential conflict of interest.

Publisher's note

All claims expressed in this article are solely those of the authors and do not necessarily represent those of their affiliated organizations, or those of the publisher, the editors and the reviewers. Any product that may be evaluated in this article, or claim that may be made by its manufacturer, is not guaranteed or endorsed by the publisher.

References

- Kanis JA, Cooper C, Rizzoli R, Reginster JY. Scientific Advisory Board of the European Society for Clinical and Economic Aspects of Osteoporosis and Osteoarthritis (ESCEO) and the Committees of Scientific Advisors and National Societies of the International Osteoporosis Foundation (IOF). Executive summary of the European guidance for the diagnosis and management of osteoporosis in postmenopausal women. *Calcif Tissue Int* (2019) 104(3):235–38. doi: 10.1007/s00223-018-00512-x
- Kanis JA, Cooper C, Rizzoli R, Reginster JY. Scientific Advisory Board of the European Society for Clinical and Economic Aspects of Osteoporosis (ESCEO) and the Committees of Scientific Advisors and National Societies of the International Osteoporosis Foundation (IOF). European guidance for the diagnosis and management of osteoporosis in postmenopausal women. *Osteoporos Int* (2019) 30(1):3–44. doi: 10.1007/s00198-018-4704-5
- Armas LA, Recker RR. Pathophysiology of osteoporosis: new mechanistic insights. *Endocrinol Metab Clin North Am* (2012) 41(3):475–86. doi: 10.1016/j.ecl.2012.04.006
- Tominaga A, Wada K, Okazaki K, Nishi H, Terayama Y, Kato Y, et al. Early clinical effects, safety, and predictors of the effects of romosozumab treatment in osteoporosis patients: one-year study. *Osteoporos Int* (2021) 32(10):1999–2009. doi: 10.1007/s00198-021-05925-3
- Ziegler R. Osteoporose–diagnose und therapie [Osteoporosis–diagnosis and therapy]. *Med Klin (Munich)* (1996) 91 Suppl 1:29–33.
- Watts NB, Camacho PM, Lewiecki EM, Petak SMAACE/ACE Postmenopausal Osteoporosis Guidelines Task Force. American Association of clinical Endocrinologists/American college of endocrinology clinical practice guidelines for the diagnosis and treatment of postmenopausal osteoporosis-2020 update. *Endocr Pract* (2021) 27(4):379–80. doi: 10.1016/j.eprac.2021.02.001
- Management of osteoporosis in postmenopausal women. *The 2021 position statement of The North American Menopause Society. Menopause* (2021) 28(9):973–97. doi: 10.1097/GME.0000000000001831
- Yong EL, Logan S. Menopausal osteoporosis: screening, prevention and treatment. *Singapore Med J* (2021) 62(4):159–66. doi: 10.11622/smedj.2021036
- Zhang ND, Han T, Huang BK, Rahman K, Jiang YP, Xu HT, et al. Traditional Chinese medicine formulas for the treatment of osteoporosis: Implication for

- antiosteoporotic drug discovery. *J Ethnopharmacol* (2016) 189:61–80. doi: 10.1016/j.jep.2016.05.025
10. Chen SQ, Liang W, Zhang XM, Li X, Zhan ZL, Guo LP, et al. [Research progress on chemical compositions and pharmacological action of drynariae rhizoma]. *Zhongguo Zhong Yao Za Zhi* (2021) 46(11):2737–45. doi: 10.19540/j.cnki.cjcm.20210222.602
 11. Jiang YC, Li YF, Zhou L, Zhang DP. UPLC-MS metabolomics method provides valuable insights into the effect and underlying mechanisms of rhizoma drynariae cataplasm on fracture healing in a rat model of osteoporosis. *Med Sci Monit* (2020) 1152:122262. doi: 10.1016/j.jchomb.2020.122262
 12. Hu Y, Mu P, Ma X, Shi J, Zhong Z, Huang L. Rhizoma drynariae total flavonoids combined with calcium carbonate ameliorates bone loss in experimentally induced osteoporosis in rats via the regulation of Wnt3a/ β -catenin pathway. *J Orthop Surg Res* (2021) 16(1):702. doi: 10.1186/s13018-021-02842-3
 13. Guo W, Shi K, Xiang G, Lu D, Dou H, Xie C, et al. Effects of rhizoma drynariae cataplasm on fracture healing in a rat model of osteoporosis. *Med Sci Monit* (2019) 25:3133–9. doi: 10.12659/MSM.914568
 14. Lin J, Zhu J, Wang Y, Zhang N, Guber HJ, Qiu X, et al. Chinese Single herbs and active ingredients for postmenopausal osteoporosis: From preclinical evidence to action mechanism. *Biosci Trends* (2017) 11(5):496–506. doi: 10.5582/bst.2017.01216
 15. Gan D, Xu X, Chen D, Feng P, Xu Z. Network pharmacology-based pharmacological mechanism of the Chinese medicine rhizoma drynariae against osteoporosis. *Med Sci Monit* (2019) 25:5700–16. doi: 10.12659/MSM.915170
 16. Chen SH, Wang XL, Zheng LZ, Dai Y, Zhang JY, Guo BL, et al. Comparative study of two types of herbal capsules with different Epimedium species for the prevention of ovariectomized-induced osteoporosis in rats. *J Orthop Translat* (2015) 4:14–27. doi: 10.1016/j.jot.2015.07.001
 17. Yan L, Zhihang L, Yungang C, Weilong R, Haipeng X, Zhanfang X, et al. Effect of drynaria decoction on adipogenic differentiation of bone marrow mesenchymal stem cells in ovariectomized osteoporosis rats via wnt/ β -catenin pathway influence. *Chin J Tradit Chin Med* (2019) 37(02):279–284+518–520. doi: 10.13193/j.issn.1673-7717.2019.02.004
 18. Lina Z, Xuxia W, Wenjuan Z, Yuan W, Jun Z. Effects of drynaria decoction on osteoclasts during orthodontic tooth movement in rats. *Shanghai J Tradit Chin Med* (2011) 45(06):72–5. doi: 10.16305/j.1007-1334.2011.06.023
 19. Blanchard OL, Smoliga JM. Translating dosages from animal models to human clinical trials—revisiting body surface area scaling. *FASEB J* (2015) 29(5):1629–34. doi: 10.1096/fj.14-269043
 20. Xiongfai H, Zhilian C, Shu Y. Meta-analysis of anesthesia effect of sodium pentobarbital and chloral hydrate on rats. *J Toxicol* (2020) 34(03):208–13. doi: 10.16421/j.cnki.1002-3127.2020.03.006
 21. Yu X, Chen S, OL P, SM M, Li J, JM P, et al. Neurofibromin and its inactivation of ras are prerequisites for osteoblast functioning. *Bone* (2005) 36(5):793–802. doi: 10.1016/j.bone.2005.01.022
 22. Papaioannou G, Mirzamohammadi F, Kobayashi T. Ras signaling regulates osteoprogenitor cell proliferation and bone formation. *Cell Death Dis* (2016) 7(10):e2405. doi: 10.1038/cddis.2016.314
 23. Peng H, Yu Y, Gu H, Qi B, Yu A. MicroRNA-483-5p inhibits osteogenic differentiation of human bone marrow mesenchymal stem cells by targeting the RPL31-mediated RAS/MEK/ERK signaling pathway. *Cell Signal* (2022) 3:110298. doi: 10.1016/j.cellsig.2022.110298
 24. Chen L, Shi X, Xie J, Weng SJ, Xie ZJ, Tang JH, et al. Apelin-13 induces mitophagy in bone marrow mesenchymal stem cells to suppress intracellular oxidative stress and ameliorate osteoporosis by activation of AMPK signaling pathway. *Free Radic Biol Med* (2021) 163:356–68. doi: 10.1016/j.freeradbiomed.2020.12.235
 25. Han XF, Zhang XX, Liu KM, Zhang Q. Apelin-13 deficiency alters cortical bone geometry, organic bone matrix, and inhibits wnt/ β -catenin signaling. *Gen Comp Endocrinol* (2018) 267:29–35. doi: 10.1016/j.ygcen.2018.05.024
 26. Solà-Vilà D, Dilmé JF, Rodríguez C, Soto B, Vila L, Escudero JR, et al. Expression and cellular localization of 15-Hydroxy-Prostaglandin-Dehydrogenase in abdominal aortic aneurysm. *PLoS One* (2015) 10(8):e0136201. doi: 10.1371/journal.pone.0136201
 27. Adami G, Fassio A, Rossini M, Caimmi C, Giollo A, Orsolini G, et al. Osteoporosis in rheumatic diseases. *Int J Mol Sci* (2019) 20(23):5867. doi: 10.3390/ijms20235867
 28. Pirsil F, Curtis LM, Steinberg SM, Tella SH, Katić M, Dobbin M, et al. Characterization and risk factor analysis of osteoporosis in a Large cohort of patients with chronic graft-versus-Host disease. *Biol Blood Marrow Transplant* (2016) 22(8):1517–24. doi: 10.1016/j.bbmt.2016.04.012
 29. Kitaura H, Marahleh A, Ohori F, Noguchi T, Shen WR, Qi J, et al. Osteocyte-related cytokines regulate osteoclast formation and bone resorption. *Int J Mol Sci* (2020) 21(14):5169. doi: 10.3390/ijms21145169
 30. Feng X. Regulatory roles and molecular signaling of TNF family members in osteoclasts. *Gene* (2005) 350(1):1–13. doi: 10.1016/j.gene.2005.01.014
 31. Plotnikov SV, Pasapera AM, Sabass B, Waterman CM. Force fluctuations within focal adhesions mediate ECM-rigidity sensing to guide directed cell migration. *Cell* (2012) 151:1513–27. doi: 10.1016/j.cell.2012.11.034
 32. Bao Y, Wang L, Shi L, Yun F, Liu X, Chen Y, et al. Transcriptome profiling revealed multiple genes and ECM-receptor interaction pathways that may be associated with breast cancer. *Cell Mol Biol Lett* (2019) 24:38. doi: 10.1186/s11658-019-0162-0
 33. Wang C, Yu T, Tan L, Cheng J. Bioinformatics analysis of gene expression profile in callus tissues of osteoporotic phenotype mice induced by osteoblast-specific Krm2 overexpression. *Int J Rheum Dis* (2016) 19(12):1263–71. doi: 10.1111/1756-185X.12840
 34. Xiong Y, Cao F, Chen L, Yan C, Zhou W, Chen Y, et al. Identification of key microRNAs and target genes for the diagnosis of bone nonunion. *Mol Med Rep* (2020) 21(4):1921–33. doi: 10.3892/mmr.2020.10996
 35. Winter EM, Kooijman S, Appelman-Dijkstra NM, Meijer OC, Rensen PC, Schilperoort M. Chronobiology and chronotherapy of osteoporosis. *JBM Plus* (2021) 5(10):e10504. doi: 10.1002/jbm4.10504
 36. Fujihara Y, Kondo H, Noguchi T, Togari A. Glucocorticoids mediate circadian timing in peripheral osteoclasts resulting in the circadian expression rhythm of osteoclast-related genes. *Bone* (2014) 61:1–9. doi: 10.1016/j.bone.2013.12.026
 37. Yi CH, Zheng T, Leaderer D, Hoffman A, Zhu Y. Cancer-related transcriptional targets of the circadian gene NPAS2 identified by genome-wide ChIP-on-chip analysis. *Cancer Lett* (2009) 284(2):149–56. doi: 10.1016/j.canlet.2009.04.017
 38. Yang T, Yuan P, Yang Y, Liang N, Wang Q, Li J, et al. NPAS2 contributes to liver fibrosis by direct transcriptional activation of Hes1 in hepatic stellate cells. *Mol Ther Nucleic Acids* (2019) 18:1009–22. doi: 10.1016/j.omtn.2019.10.025
 39. Morinaga K, Sasaki H, Park S, Hokugo A, Okawa H, Tahara Y, et al. Neuronal PAS domain 2 (Npas2) facilitated osseointegration of titanium implant with rough surface through a neuroskeletal mechanism. *Biomaterials* (2019) 192:62–74. doi: 10.1016/j.biomaterials.2018.11.003
 40. Kunimoto T, Okubo N, Minami Y, Fujiwara H, Hosokawa T, Asada M, et al. A PTH-responsive circadian clock operates in *ex vivo* mouse femur fracture healing site. *Sci Rep* (2016) 6:22409. doi: 10.1038/srep22409
 41. Zheng J, Zhang L, Tan Z, Zhao Q, Wei X, Yang Y, et al. Bmal1- and Per2-mediated regulation of the osteogenic differentiation and proliferation of mouse bone marrow mesenchymal stem cells by modulating the wnt/ β -catenin pathway [published online ahead of print, 2022 Apr 6]. *Mol Biol Rep* (2022). doi: 10.1007/s11033-022-07292-6
 42. Tang Z, Xu T, Li Y, Fei W, Yang G, Hong Y. Inhibition of CRY2 by STAT3/miRNA-7-5p promotes osteoblast differentiation through upregulation of CLOCK/BMAL1/P300 expression. *Mol Ther Nucleic Acids* (2020) 19:865–76. doi: 10.1016/j.omtn.2019.12.020
 43. Takahashi S, Inoue I, Nakajima Y, Seo M, Nakano T, Yang F, et al. A promoter in the novel exon of hPPARgamma directs the circadian expression of PPARgamma. *J Atheroscler Thromb* (2010) 17(1):73–83. doi: 10.5551/jat.2410
 44. Yang Y, van Meurs JB, Arp P, van Leeuwen JP, Hofman A, Pols HA, et al. Vitamin d binding protein genotype and osteoporosis. *Calcif Tissue Int* (2009) 85(2):85–93. doi: 10.1007/s00223-009-9251-9
 45. Mulloy B, Rider CC. The bone morphogenetic proteins and their antagonists. *Vitam Horm* (2015) 99:63–90. doi: 10.1016/bs.vh.2015.06.004
 46. Feng Y, Zhu L, Gu Y, Wang LJ, Niu BJ, Cai F, et al. Association of gremlin-2 gene polymorphisms with osteoporosis risk in Chinese postmenopausal women. *Biosci Rep* (2020) 40(4):BSR20200554. doi: 10.1042/BSR20200554
 47. Suzuki D, Yamada A, Aizawa R, Funato S, Matsumoto T, Suzuki W, et al. BMP2 differentially regulates the expression of Gremlin1 and Gremlin2, the negative regulators of BMP function, during osteoblast differentiation. *Calcif Tissue Int* (2012) 91(1):88–96. doi: 10.1007/s00223-012-9614-5
 48. Schmideithner L, Thabet Y, Schönfeld E, Köhne M, Sommer D, Abdullah Z, et al. Enzymatic activity of HPGD in treg cells suppresses tconv cells to maintain adipose tissue homeostasis and prevent metabolic dysfunction. *Immunity* (2019) 50(5):1232–48.e14. doi: 10.1016/j.immuni.2019.03.014
 49. Eiraku M, Tohgo A, Ono K, Kaneko M, Fujishima K, Hirano T, Kaneko M, Fujishima K, Hirano T, et al. DNER acts as a neuron-specific notch ligand during bergmann glial development. *Nat Neurosci* (2005) 8:873–80. doi: 10.1038/nn1492
 50. Park JR, Jung JW, Seo MS, Kang SK, Lee YS, Kang KS. DNER modulates adipogenesis of human adipose tissue-derived mesenchymal stem cells via regulation of cell proliferation. *Cell Prolif* (2010) 43(1):19–28. doi: 10.1111/j.1365-2184.2009.00650.x
 51. Lv S, Wang N, Ma J, WP L, ZJ C, Zhang C. Impaired decidualization caused by downregulation of circadian clock gene BMAL1 contributes to human recurrent miscarriage. *Biol Reprod* (2019) 101(1):138–47. doi: 10.1093/biolre/iz0063

52. Wang Z, Li Z, Wu Q, Li C, Li J, Zhang Y, et al. DNER promotes epithelial-mesenchymal transition and prevents chemosensitivity through the wnt/ β -catenin pathway in breast cancer. *Cell Death Dis* (2020) 11(8):642. doi: 10.1038/s41419-020-02903-1

53. Hanson RL, Muller YL, Kobes S, Guo T, Bian L, Ossowski V, et al. A genome-wide association study in American indians implicates DNER as a

susceptibility locus for type 2 diabetes. *Diabetes* (2014) 63(1):369–76. doi: 10.2337/db13-0416

54. Asadipooya K, Uy EM. Advanced glycation end products (AGEs), receptor for AGEs, diabetes, and bone: Review of the literature. *J Endocr Soc* (2019) 3(10):1799–818. doi: 10.1210/js.2019-00160